EVS30 Symposium
Stuttgart, Germany, October 9 - 11, 2017

Winter testing of electric in-wheel motors

Gorazd Gotovac[1], Blaž Modic[1], Primož Tominc[1], Uroš Rožič[1], Tomaž Motaln[1]

[1]*Elaphe Propulsion Technologies, Teslova ulica 30, 1000 Ljubljana, Slovenia, gorazd.gotovac@elaphe-ev.com*

Summary

This paper presents an overview of in-wheel electric motor winter testing, including test execution and testing results. Three testing topics are presented, namely traction control testing, NVH testing and driving cycle testing, representing broader test groups of vehicle dynamics, durability and environmental testing respectively. The tests are presented on an example of testing a 2WD and a 4WD vehicle, both using in-wheel motors as their sole powertrain, in winter conditions of Heihe, China winter testing center. The traction control tests were focused on tuning and validation of the maximum transmissible torque algorithm implemented on the Elaphe™ "Propulsion control unit" ("PCU"). The available testing surfaces include compacted snow, smooth snow, ice, tarmac and their combinations. The NVH section describes the selected road surface conditions for testing the in-wheel motor, including potholes, brick road, embedded rock, and others and presents the obtained loads (accelerations on the critical motor parts) and other observed potential failure modes. Finally, the driving cycle testing is shown as an example of tests that simulate normal vehicle use in winter conditions in order to detect functionality issues, learn about system behavior and gather data about environmental impact on the system components. In conclusion, testing in winter conditions provides an indispensable source of data to improve reliability, functions and performance of the in-wheel electric powertrain, proving its reliability in the most demanding conditions.

Keywords: wheel hub motor, efficiency, regenerative braking, traction control, testing processes,

1 Introduction

The automotive environmental and load requirements are among the toughest of any market for electric powertrains. When a powertrain motor is placed inside the wheel of a vehicle, these requirements are amplified and the toughest testing conditions need to be selected in order to guarantee reliable operation throughout the motor lifetime. Conditions inside the wheel of a vehicle feature a large temperature span ranging from -40°C up to 85°C, vibrations with large amplitudes and direct exposure to agents such as water, mud, ice, gravel and chemicals present on the road. A big part of the endurance requirement for such an in-wheel motor comes from winter use of vehicles. Extremely cold weather and winter conditions can produce dimensional changes of structural parts, change in material elasticity and toughness, induce corrosion of critical components and potentially even cause failure of the insulation system. In addition, ensuring safety in winter conditions requires fine tuning of the vehicle dynamic behavior in low friction conditions.

In order to validate how the in-wheel motor system behaves in these kind of conditions, winter testing was performed at the Red Valley Proving Grounds in the northern Chinese city of Heihe, in temperatures ranging from below -30°C up to -10°C. The following paper presents some of the most interesting tests and obtained results of their influence on in-wheel motors. The tests were performed by testing a 2-wheel drive and a 4-wheel drive vehicle, both using in-wheel motors as their sole electric powertrain.

2 Traction control

Low adhesion surfaces, found on winter testing tracks, are ideal for testing traction control. Using in-wheel motors provides complete traction independence for each powered wheel and offers potential for the use of advanced wheel slip control algorithms. Several approaches can be used [1–3], requiring only software implementation without the use of advanced mechanical differentials.

The maximum transmissible torque estimation algorithm [2] that was implemented on the test vehicle, is used to limit the output torque based on the ratio of the actual wheel acceleration versus the expected acceleration of the vehicle in presence of the applied torque. However, in order not to decrease the acceleration performance, other algorithms were developed and implemented to prevent the traction control system from limiting the motors torque in high traction surfaces.

2.1 Used algorithm

The use of in-wheel motors reduces the need for complex mechanical systems like limited slip differential, since they provide complete traction independence for each powered wheel and so offer the potential for the use of advanced traction control algorithms. Wheel slip λ in both acceleration and deceleration is defined in (1) using wheel and vehicle speed.

$$\lambda = \begin{cases} \frac{v_{wheel} - v_{vehicle}}{v_{wheel}}, & v_{wheel} > v_{vehicle} \\ \frac{v_{whe} - v_{vehicle}}{v_{vehicle}}, & v_{wheel} < v_{vehicle} \end{cases} \quad (1)$$

Since an electric vehicle can be both accelerated and decelerated by using its electric motors, the traction of the wheels can be controlled in both situations. During acceleration, wheel slip is controlled by using the traction control (TRC) system, and during braking, an analogue algorithm called anti-lock regenerative braking system (ARBS) is used. Among other options, the maximum transmissible torque approximation algorithm (MTTA) [2] was used because of its ability to be integrated on vehicles with different propulsion system configurations without performing extensive tuning for each separate vehicle. The algorithm also does not require the vehicle "true speed" which is an additional benefit for four-wheel drive systems. Wheel slip is controlled by setting the maximum allowed value of α, which is the ratio between the longitudinal acceleration of the vehicle and that of the wheel (2).

$$\alpha = \frac{\frac{dv_{vehicle}}{dt}}{\frac{dv_{wheel}}{dt}} \quad (2)$$

Driving force F_d that is being applied at the contact of the tyre and the driving surface can be approximated based on the measured applied torque (T) and the resulting acceleration of the wheel (3) and taking into account the wheel inertia (J_{wheel}) and the wheel radius (r_{wheel})

$$F_d = \frac{1}{r_{wheel}} \left(T - \frac{J_{wheel} \cdot \frac{dv_{wheel}}{dt}}{r_{wheel}} \right) \quad (3)$$

If no wheel slip occurs, the acceleration of the wheel is low and the driving force is defined mostly with the applied torque and the radius of the wheel. However, if extensive wheel slip occurs, the wheel acceleration increases, which decreases the driving force and the applied torque needs to be reduced. Previously mentioned parameter α and other parameters of the vehicle define the extent to which the applied torque is reduced (4).

$$T_{max} = \left(\frac{J_{wheel}}{\alpha \cdot m_{vehicle} \cdot r_{wheel}^2} + 1 \right) \cdot r_{wheel} \cdot F_d \quad (4)$$

The equations described above describe the MTTA algorithm while accelerating, where wheel slip is defined in the upper part of equation (1). For braking, the equations need to be slightly modified.

In order not to decrease the acceleration and braking performance, other algorithms were also developed and implemented to prevent the TRC and ARBS from limiting the motors torque in good traction conditions.

2.2 Algorithm tuning

Testing of the algorithms was performed on several different surfaces in order to tune the algorithm for optimal use in winter conditions. The tests were performed on an in-wheel powered BAIC EV260 vehicle. Good adhesion scenarios were represented by tarmac and by compacted snow, which both offered excellent grip in very cold conditions. Poor traction conditions were represented by smoothened snow and by ice, which offered very little grip. Finally, testing was also performed on mixed surfaces, either by positioning some of the traction wheels on good and some on poor grip surfaces or by changing the surface during acceleration or braking. Some of the test conditions are presented in Figure 1 and Figure 2.

Figure 1: Test vehicle on a mixed surface

Figure 2: Test vehicle on compacted snow

Since the speed of the vehicle was measured only indirectly through the speed of the wheels, the actual speed of the vehicle was not known when wheel slip or blocking occurred. This meant that the algorithms had to be tuned by comparing the response of the vehicle to the same drive inputs at different settings of the algorithm parameters, as is presented on an example of one of the model parameters in Figure 3 and Figure 4.

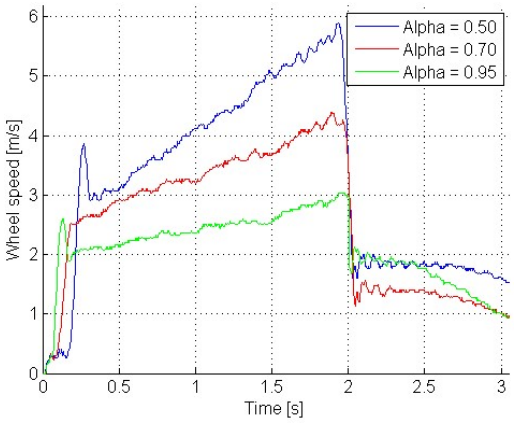

Figure 3: Speed response of the in-wheel motor during full torque request on a low adhesion surface at different settings of alpha TRC parameter.

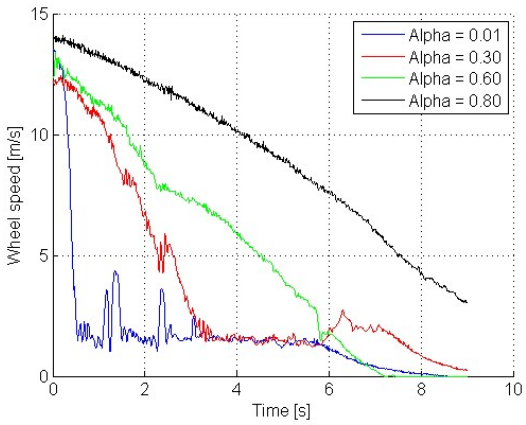

Figure 4: Speed response of the in-wheel motor during full regenerative braking request on a low adhesion surface at different settings of ARBS alpha parameter.

In this way, the influence of each parameter on the performance of the TRC and ARBS algorithms was determined and at the end, the parameters were set in a way that best performance both in low and high traction conditions was obtained.

After tuning, both algorithms needed to be validated. Validation tests were performed on different driving surfaces. Each test was executed multiple times with the vehicle advanced traction control algorithm disabled

and enabled. It was checked whether acceleration and braking performance along with the stability of the vehicle were improved if the vehicle dynamics algorithms were activated.

2.3 Validation tests

The TRC algorithm validation tests were performed first. Acceleration tests on dry tarmac, snow, ice, and mixed surface were executed. The following three scenarios were tested on each surface:

1. TRC was disabled and driver was allowed to release the throttle pedal if he detected wheel slip
2. TRC was disabled and the driver never released the throttle pedal
3. TRC was enabled and the driver never released the throttle pedal

Speed of both in-wheel motors alongside with the applied torque in all three scenarios during acceleration on mixed surface, where the left wheel was positioned on dry tarmac and the right one on ice, are presented in Figure 5, Figure 6, and Figure 7.

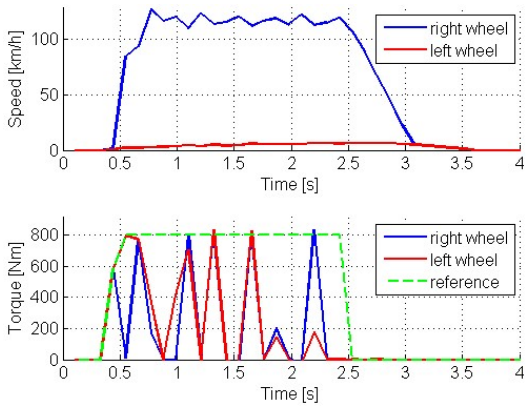

Figure 5: Mixed surface acceleration test with TRC disabled. The driver never released the throttle pedal.

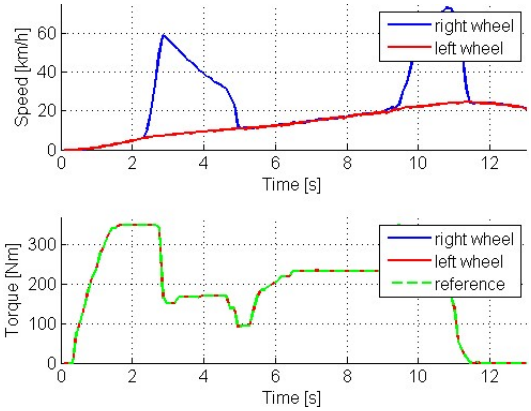

Figure 6: Mixed surface acceleration test with TRC disabled. The driver released the throttle pedal if he detected wheel slip.

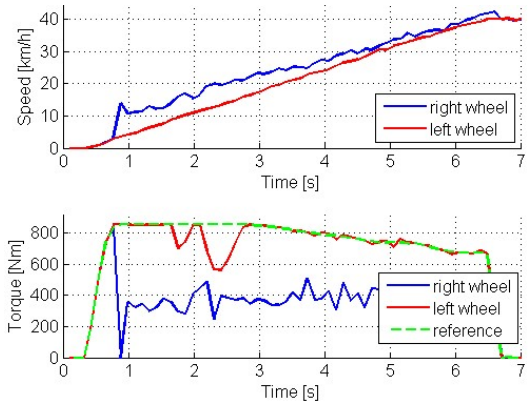

Figure 7: Mixed surface acceleration test with TRC enabled. The driver never released the throttle pedal.

It can be seen that when TRC was disabled, extensive wheel slip was present on the wheel with low traction. Improvements in acceleration time caused by the activation of the TRC algorithm when accelerating from 0 to 40 km/h on different driving surfaces is presented in Table 1.

The stability of the vehicle was observed in tests where the driving surfaces changed from very high (dry tarmac) to very low (ice) adhesion. The stability of the vehicle was greatly improved when TRC was enabled and no loss of the vehicles control was detected during all tests, while the vehicle spun out of control during some tests when TRC was disabled.

Table 1: Acceleration time improvements when TRC was enabled on different driving surfaces

Driving surface	Ice	Snow	Mixed
Acceleration time decrease	42%	36%	65%

Tuning of the ARBS algorithm followed. Similar to the TRC tests, the braking performance with ARBS disabled and enabled on different driving surfaces was tested. During all the tests, only regenerative braking was used and the mechanical brakes were never activated. Speed of both in-wheel motors alongside with the applied torque during braking on snow with ARBS disabled and enabled were recorded and are displayed in Figure 8 and Figure 9 respectively.

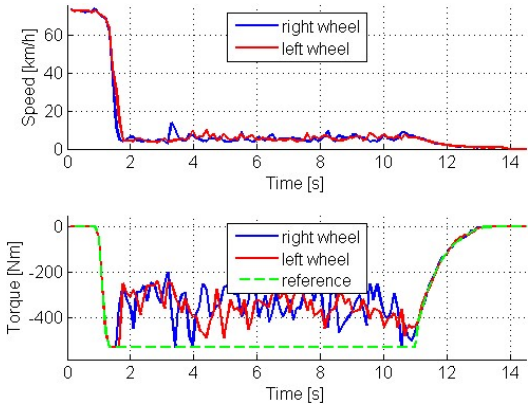

Figure 8: Speed and torque of both in-wheel motors while braking on snowy surface with ARBS disabled.

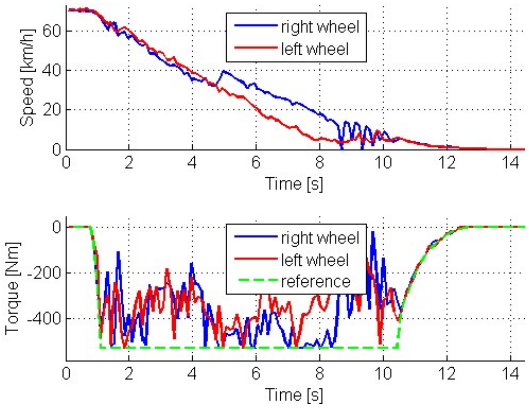

Figure 9: Speed and torque of both in-wheel motors while braking on snowy surface with ARBS enabled.

It can be seen that severe wheel blocking and sometimes even backspin (in very low adhesion conditions) occurs when regenerative braking is applied, if ARBS is not enabled. On the other hand, when ARBS is enabled, it successfully reduces the motor torque to prevent wheel blocking and therefore substantially increases the stability of the vehicle. Both braking distance and time are decreased when ARBS is active and are presented in Table 2.

Table 2: Stopping time and distance for braking from 50 km/h to standstill on a snowy surface if ARBS is enabled or disabled.

	Stopping time [s]	Stopping distance [m]
ARBS disabled	10.33	71.5
ARBS enabled	9.01	62.5

The ability of the ARBS algorithm to quickly adapt to sudden changes of the driving surfaces friction coefficient was tested in the scenario, presented in Figure 10.

Only regenerative braking was applied while driving on ice. After some time, the driving surface suddenly changed to dry tarmac with high friction coefficient. Operation of both in-wheel motors during this test can be observed in Figure 11.

It can be seen that the surfaces changed approximately 1 second after braking was initiated. This increased the maximum braking force that could be applied without blocking the wheel, which was successfully detected by the ARBS algorithm and regeneration torque was quickly increased from around 300 Nm to 480 Nm per wheel, which was set as the maximum allowed regeneration motor torque.

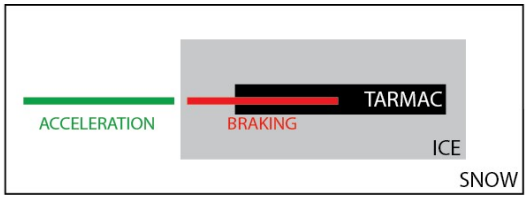

Figure 10: Change of driving surfaces test scenario

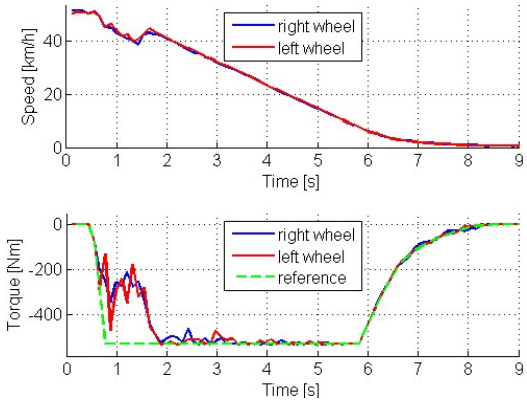

Figure 11: Speed and torque of both in-wheel motors when driving surface suddenly changed from ice to dry tarmac.

The validation tests show the successful implementation of advanced traction control algorithms on a vehicle with in-wheel motor powertrain technology. Such implementation is simple and does not require any hardware modification and is thus a great advantage of a distributed direct drive powertrain.

3 NVH testing

In-wheel motors are mounted inside the vehicles wheel and integrated on the vehicle. Unlike central engines where vehicle chassis provides protection against environmental hazards the in-wheel motors are directly exposed to harsh structural and environmental conditions like extreme temperatures and severe loading. In order to guaranty reliability and durability, in-wheel motors are lead through series of extremely harsh tests where accelerations can reach up to 100G. Damage due to this severe loading is even greater when performed in extreme weather conditions. To mimic such environment a winter testing session in Northern China was set up. Test field was prepared on a frozen river where temperatures reached down to -40°C. The surfaces used in testing (Figure 12) can be found in international standards [4], automotive requirements and track specifications [5].

Figure 12: Examples of testing surfaces: Belgian block road, potholes, waves, embedded rocks, bricks, speed bumps

The goal of these tests was to check the operation of Elaphe M700 motors in a very harsh environment with high external loading. Besides that, the goal was also to measure useful values for later durability evaluation of our motors. Test vehicle used two in-wheel M700 motors and was equipped with three-axis accelerometer

which was positioned on the stator of M700 motor (Figure 14). Vibrations were captured with high speed DAQ with purpose to be evaluated and replicated also on shakers for comprehensive durability testing. Test track represented eight different track surfaces and among all test loops the one with highest amplitudes was analysed in detail. In addition to the special track evaluations, high speed driving on a rough road was performed to obtain expected "normal" harsh use scenario values (example in Figure 13)

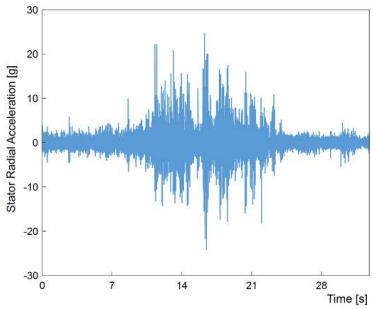

Figure 13: Stator radial accelerations when driving with 90 km/h over a rough road

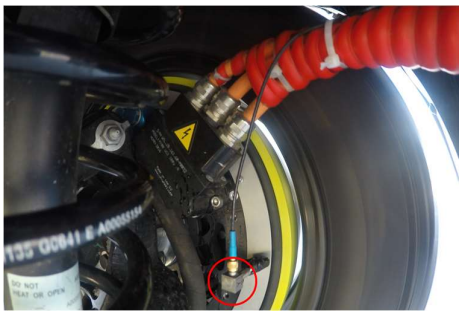

Figure 14: Accelerometer positioning on the stator of the M700 in-wheel motor

3.1 Analysis

The tests were captured and analysed already during measurements by using Dewesoft vibration measurement equipment and software (Figure 15). Among all the performed tests the highest recorded acceleration amplitudes were 36 G in vertical and 33 G in longitudinal direction. The most interesting measurements are presented below.

Measurements were processed with Fast Fourier Transform algorithm (FFT) which revealed the vibration frequency peaks. Three peaks are visible in Figure 16 – the first peak at 9.49 Hz is direct response of track vibrations and peaks at 320Hz and 500Hz are frequency responses of the stator structure itself.

Figure 15: Online analysis of the stator vibrations

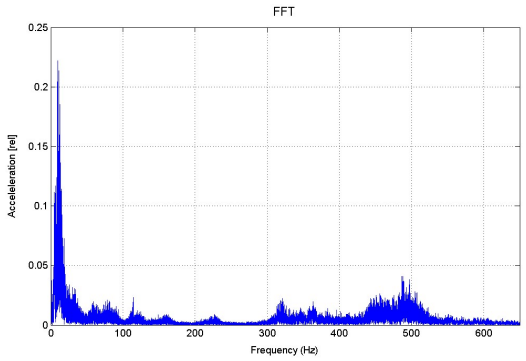

Figure 16: FFT analysis of vibrations

To confirm that the second and third peak are really the response of the stator, modal analysis using FEM was performed. Both mode shapes that are excited, can be seen on Figures 16 and 17. Mode shape on the figure 16 is directly excited with accelerations from the road and the mode shape on the Figure 17 is the result of the vibration due to the excitation torque of the motor. Further on, accelerations from one test loop were plotted in terms of Power Spectral Density (PSD) graph Figure 18. Peaks at 320Hz and 500Hz can be well identified from the graph.

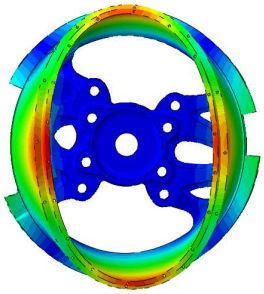

Figure 17: Mode shape at 322Hz

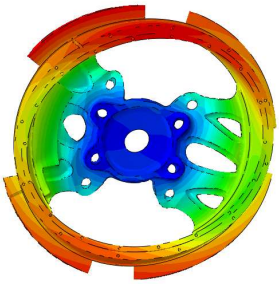

Figure 18: Mode shape at 492Hz

On the Figure 18 we can also see the direct comparison between the measured PSD on the NVH road and the ISO 16750-3:2007(E) standard. This is the standard for random vibration profile used for accelerated evaluating the durability unsprung parts of the vehicle, so laboratory tests and fatigue simulations are performed using this profile Figure 19.

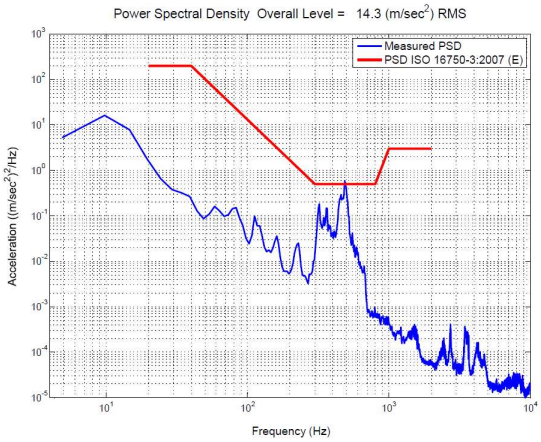

Figure 19: PSD spectrum of vibrations in vertical direction. Red line represents test profile according to ISO 16750-3:2007(E)

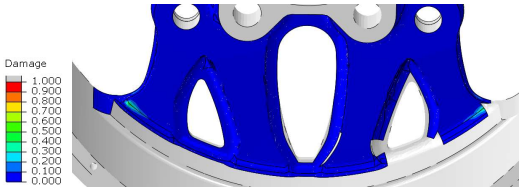

Figure 20: FEM analysis of the fatigue Damage

The RMS value of the acceleration for the measured signal was $14{,}3m/s^2$ while ISO 16750-3:2007(E) has RMS value of $107{,}3m/s^2$ since the ISO profile is meant for accelerated testing. This means that the ISO profile is a lot harsher comparing to what we measured on the NVH road. Moreover the driving on the NVH road lasted only 40s while ISO standard lasts for 24h.

By using equation for accelerated testing [6] it was recalculated that test vehicle could drive at test track for roughly 1350 hours to experience the same vibration intensity as it would during 24 hours of ISO laboratory testing. 1350 hours sounds a lot but with consideration that entire test track with different surfaces and connection paths in between was taken into account the value is reasonable. Part of the track with highest measured acceleration RMS was resonance road with RMS value of $49{,}5m/s^2$. If only this part of testing track is compared against ISO standard then the vehicle could drive for 110 hours on this section to experience the same vibration intensity as in ISO standard. Test velocity was $24km/h$ and in 110 hours vehicle would cover the distance of $2640km$.

4 Driving cycle testing

Besides the systematic testing of system functionality and vibration on the in-wheel motor, testing system behavior during long term exposure to winter conditions is also very important. Therefore, cycle tests, lasting several hours, were performed. They showed the typical state of the system in such conditions, offering insight into potential improvements and failure modes of the system. Characterization of the system before, after, and also during a given cycle is key to quantifying the system status and potential indications of trends that might lead to failure modes.

The focus of this paper however, is the behaviour of the powertrain energy flow, in comparison to the simulated data based on the driving cycle log. The presented driving cycle was recorded on a 2.5 hour drive on local roads in Heihe area (Figure 22).

Figure 21: Heihe track in winter conditions

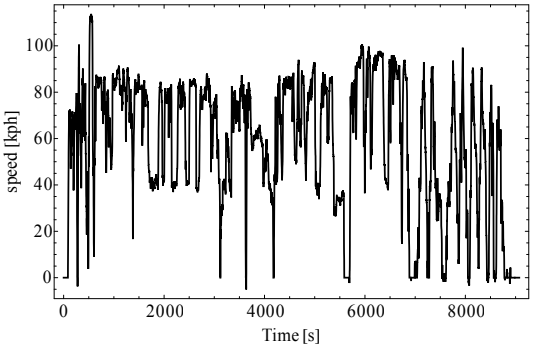

Figure 22: Recorded speed cycle during a 2.5 hour drive

The cycle can also be represented by a torque vs. speed chart, which essentially reveals the distribution of operating points within the cycle (Figure 23). The Heihe cycle is comprised out of operating points both at high speeds as well as high torques, however the dominating area is between 500 rpm and 800 rpm and within 0-200 Nm of torque. The cycle distribution itself is not important, but the comparison with simulation can give us confidence in other results of the same simulation tool.

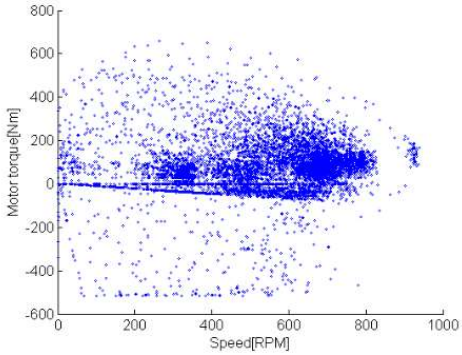

Figure 23: Distribution of wheel rotational speed and torque within the Heihe driving cycle

In order to simulate the energy consumption in the cycle, Elaphe uses in-house developed analytical tool for accurate calculation of in-wheel motor cycle efficiency and inverter efficiency. Using this tool the total consumption in any moment can be calculated according to equation (5)

$$P_{in} = P_{out} + P_{EM-loss} + P_{res} \,, \tag{5}$$

where P_{in} is the power consumption, P_{out} is the powertrain output power and $P_{EM-loss}, P_{res}$ are the electromagnetic and residual mechanical losses. Only the output power can be used for vehicle motion whereas other energy is lost before it reaches the contact of tire with road. The comparison of measured power consumption and the simulated power consumption based on the cycle speed and torque match very

well also in very dynamic conditions, such as acceleration and deceleration (Figure 24) also when the behaviour is examined more closely (Figure 25).

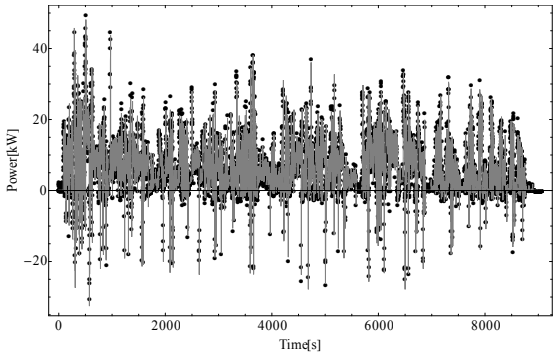

Figure 24: Comparison of measured consumed power from battery (black dots) and simulated consumed power based on the cycle torque and speed (grey curve)

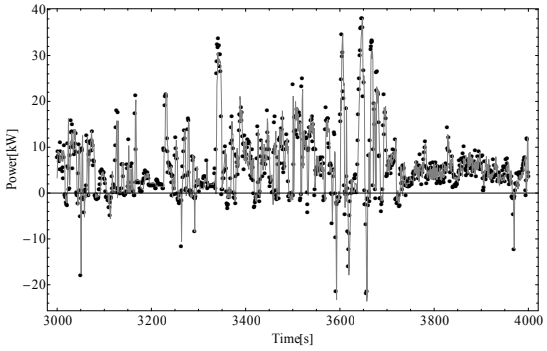

Figure 25: Close-up of a section of the cycle and comparison of measured and simulated consumption

The ultimate measure of the simulation applicability for cycle efficiency is the comparison of the average efficiency in cycle. By integrating the measured electrical power of the battery and the motor power output over time of the cycle, we obtain the overall system efficiency of 76%. At the same time the simulation output for the overall system efficiency in the Heihe cycle is 75.5%. Other cycles were checked (Figure 26) and the overall efficiency measured and calculated. The alignment in the second cycle energy efficiency is also within 1%: 84.5% measured and 83.5% calculated overall system energy efficiency.

Armed with confidence from the comparison with measured results, we can examine the simulation prediction for a standard WLTP cycle [7]. The cycle is comprised out of three basic scenarios – the urban, suburban and highway operation (Figure 27).

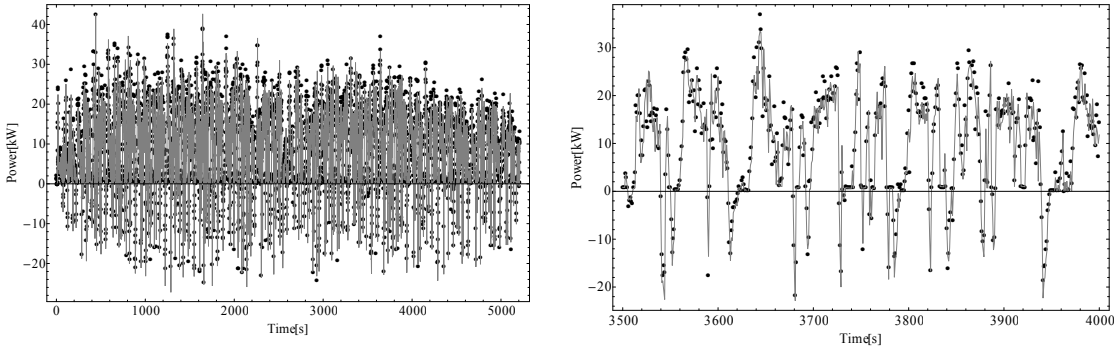

Figure 26: Example of the second Heihe cycle measurement/calculation comparison.

The torque in the standard cycle can be calculated by accounting for vehicle properties of the BAIC EV260, thus obtaining a torque vs. speed diagram (Figure 28) like in the Heihe cycle. It can be immediately observed that the WLTP cycle is much more balanced and does not favour any of the three different driving scenarios.

The same method that was used in the measured cycle case is applied to the simulation to obtain the average cycle efficiency for the WLTP cycle. When comparing just the e-Motor efficiency, it is found that the difference between cycles is quite small, only around 1% (Table 3). But, since the WLTP cycle includes more regeneration than the Heihe cycle and since the distribution of torque does not favour very low torque as much as the Heihe cycle, the overall powertrain efficiency for WLTP is higher for 6% (Table 3).

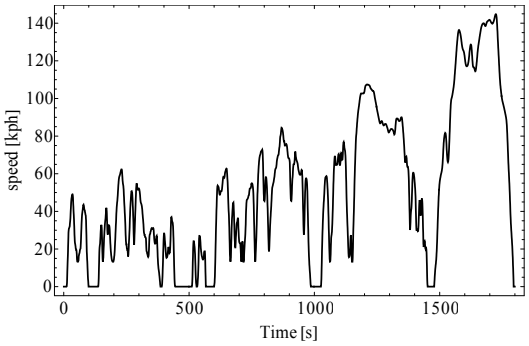

Figure 27: WLTP speed cycle used for simulation

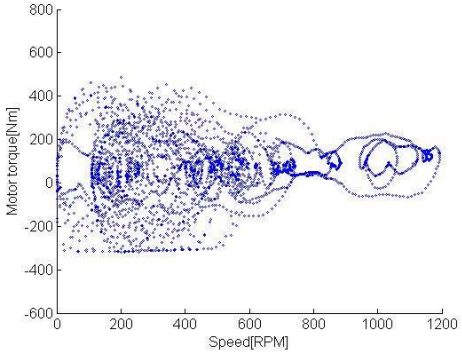

Figure 28: Distribution of wheel rotational speed and torque within the WLTP driving cycle for BAIC EV260

Table 3: Comparison of efficiencies in Heihe and WLTP cycles

	Heihe cycle 1	Heihe cycle 2	WLTP
e-Motor average efficiency	87%	90%	88%
Overall powertrain efficiency	76%	84%	82%

The cycle analysis shows good predictability of overall powertrain efficiency and potential for improvement of system efficiency by influencing the residual mechanical and electromagnetic losses, especially in low torque cycles.

5 Conclusion

Winter testing of in-wheel electric motors has shown that the in-wheel motor propulsion system can be used reliably in the most demanding winter conditions, offers great potential in vehicle dynamics control and can bear the expected loads of a rough driving surface. Continuous testing, including summer conditions, provides an opportunity for systematical improvement of the system and system components.

References

[1]. Minh, N.; Minh, C. A sliding mode algorithm for antilock braking/traction control of EVs. Science & Technology Development, Vol.18, No. K6 - 2015; pp. 174–182

[2]. Yin, D.; Oh, S.; Hori, Y. A Novel Traction Control for EV Based on Maximum Transmissible Torque Estimation. IEEE Transactions on Industrial Electronics, Vol. 56, No. 6, June 2009; pp. 2086–2094

[3]. Amodeo, M.; Ferrara, A.; Terzaghi, R.; Vecchio, C. Wheel Slip Control via Second-Order Sliding-Mode Generation. IEEE Transactions on Intelligent Transportation Systems, Vol. 11, No. 1, March 2010; pp. 122–131

[4] International standard: Road vehicles - Environmental conditions and testing for electrical and electronic equipment; Part 3: Mechanical loads ISO 16750-3:2007(E); Part 4: Climatic loads 16750-4:2010(E)

[5] Nicholas V. Kissoff, P.E., Ph.D.Test Track Design & Construction at the Transportation Research Center of Ohio (TRC)

[6] Young, Dennis E., 1993, “Focused Simulation”, available from International Safe Transit Association, 1400 Abbot Rd., Suite 160, E. Lansing, MI 48823-1900, www.ista.org

[7] UNECE, Worldwide harmonized Light vehicles Test Procedure, available on 30.6.2017 at https://circabc.europa.eu/faces/jsp/extension/wai/navigation/container.jsp

Authors

Gorazd Gotovac, PhD, is the CTO of Elaphe Propulsion technologies. In his capacity as CTO he oversees the development activities in the company, including new product development, product validation and industrialization. He received his PhD in electric motor thermal and electromagnetic analysis and his bachelor degree in mathematical physics from the University of Ljubljana, Slovenia.

Blaž Modic received his B.Sc. and M.Sc. degrees in electrical engineering from the University of Ljubljana, Ljubljana, Slovenia, in 2013 and 2016, respectively. He is currently working as an embedded firmware R&D engineer at Elaphe Ltd, focusing on the development of electric motor control and advanced vehicle dynamics related firmware.

Primož Tominc, M.Sc. is a vehicle test engineer at Elaphe Ltd. His main responsibilities include preparation of testing procedures, execution of tests and analysis of results. He moved to this position after several years of experience in automotive industry at AVL GmbH. Primož studied Mechanical Engineering at University of Ljubljana. His free time is occupied by his homemade solar electric recumbent vehicle.

Uroš Rožič received his M.Sc. in mechanical engineering from the University of Cranfield in the UK in 2013 focusing on numerical simulations using Finite element method. Uroš is the head of the CAE department which is mainly responsible for analysis of the structural integrity of all the vital parts, assessment of their thermal and cooling performance and use of numerical optimization to come up with the optimal design for the application.

Tomaž Motaln received an M.Sc in electronic engineering (2008) from University of Maribor. He is the head of electronics at Elaphe Ltd. He has 7 years of experience with control algorithms and electrical system integration for electric vehicles. His responsibility are related to the hardware and software design of different electronic components required in electric powertrain system according to automotive standards including the ISO2626 functional safety standard.